EUROPEAN ORGANIZATION FOR NUCLEAR RESEARCH
CERN — AB DEPARTMENT

CERN-AB-2006-015 ATB

DYNAMIC STRUCTURAL ANALYSIS OF THE TPSG4 & TPSG6 BEAM DILUTERS

L. MASSIDDA & F. MURA

CRS4 – Centre for Advanced Studies
Research and Development in Sardinia

Y. KADI & B. BALHAN

CERN – AB Department
Geneva

Abstract

In this report we present the technical specification for the numerical model and the study of the dynamic structural behaviour of the beam diluter elements (TPSG4 & 6) protecting the extraction septum magnets (MSE & MST) in the event of an asynchronous firing of the extraction kickers (MKE).
The deposited energy densities, estimated by the high-energy particle transport code FLUKA, were converted to internal heat generation rates according to the time dependence of the extracted beam. The transient response to this thermal load was obtained by solving the power deposition and structural deformation problem by the spectral-element code ELSE.

CRS4, Cagliari, Italy
June, 2005

CRS4 S.C.ar.l.
Loc. Pixina Manna Edificio 1
C.P. n. 25-09010 Pula, Italy
Tel +39 07092501, fax +39 0709250216
http://www.crs4.it

Computational Methods for Engineering Department

Solid and Structural Mechanics Area

This document has been revised on 03 June 2005
Previous revisions are superseded and must be destroyed or clearly marked

Authors: L. Massidda, F. Mura
Checked: F. Maggio
Approved: G. Fotia

This document contains 37 pages.

Table of Contents

1. INTRODUCTION

A new extraction channel [1] is being built in the Super Proton Synchrotron (SPS) Long Straight Section 4, LSS4, to transfer proton beams to the Large Hadron Collider (LHC) and also to the CERN Neutrino to Gran Sasso (CNGS) target. The beam is extracted in a fast mode during a single turn. A “slow” closed orbit bump is applied to move the entire beam close to the septum, and then the MKE extraction kicker fires to deflect the entire beam across an extraction septum in what should be a loss-free process (for CNGS the beam is extracted in two parts using the same principle). The extraction channel must be able to accept the high brightness LHC proton beam at 450 GeV/c, and also the high intensity, large emmittance fixed target CNGS proton beam at 400 GeV/c.

Similarly, the long straight section 6, LSS6, of the Super Proton Synchrotron (SPS) at CERN [2], is used for the resonant extraction towards experiments in the West Area. After the closure of this area at the end of 2004, the straight section will be used to transfer protons at 450 GeV/c as well as ions via the 2.8 km long transfer line TI 2 to the clockwise ring of the LHC.

In both respects, the extraction system should be adequately protected against mis-steered beams.

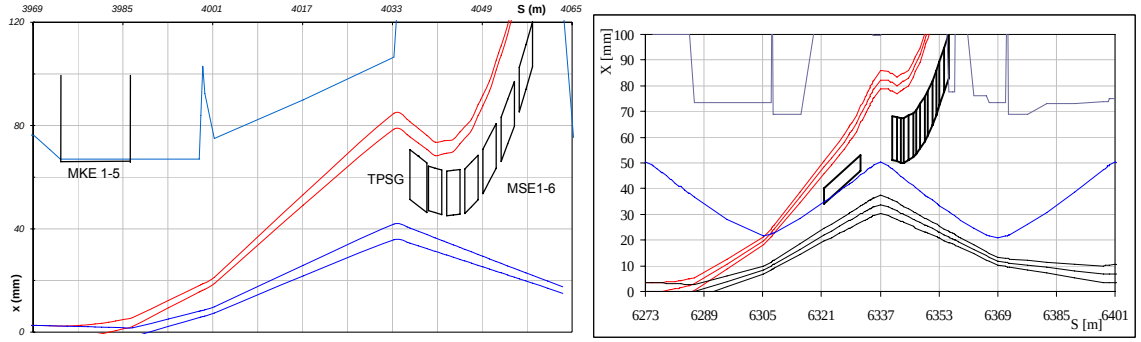

Figure 1 Schematic and functional layout of TPSG absorber system in LSS4 (left) and LSS6 (right)

The TPSG is an element designed to dilute the proton beam sufficiently to protect the copper coils of the MSE septum magnet from damage in the event of mis-steered beams at extraction [2,3,4,5]. The TPSG element is located in the extraction channel, just before the extraction septa, as illustrated in Figure 1. It should reduce the particle flux on the copper coils of the septum magnet to a safe level, such that the temperature does not exceed the chosen target value of 100 ºC in copper and 35 ºC in the cooling water.

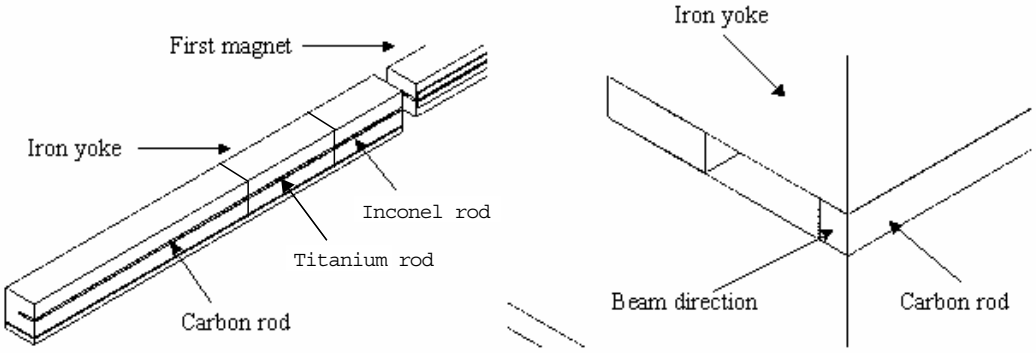

Figure 2 Schematic layout of TPSG

In the case of the LSS4 extraction channel, the TPSG4 diluter element geometry is essentially defined by the trajectories of the extracted beam, the width of the MSE septum coil (17.25 mm) plus the alignment tolerances, and the height of the MSE magnet gap (20 mm). A diluter element section of 19.25 x 30 mm^2 has been decided (Figure 2). The limited available space imposes restrictions on the total length available for the TPSG4 diluter element (a maximum of 3.0 m).

For the LSS6 extraction channel, the width of the MST septum coil is much reduced (4.2 mm), where as the height of the MST magnet gap (20 mm) is the same. A diluter element section of 6 x 30 mm^2 is considered. The limited available space imposes restrictions on the total length available for the TPSG6 diluter element (a maximum of 3.5 m).

These diluters must withstand the thermo-mechanical shock due to the energy deposited in a limited volume and in a short time by the proton beam, causing relevant stress waves propagating in the structure.

In this study these mechanical phenomena are analyzed by means of numerical simulations to assess the robustness of the target and to investigate the adequacy of the geometry and material chosen for the target elements.

1.1 OPERATING CONDITIONS

For the purpose of the analysis, the LHC ultimate beam is considered as the worst case, since the low emittance and high intensity result in a very high spatial proton density on the beam axis. The relevant nominal beam parameters are summarised in Table 1.

Table 1 Summary of the beam characteristics, diluter dimensions and other parameters assumed for the analysis (the numbers in parenthesis for the beam intensity refer to the ultimate LHC beam parameters)

Known Parameters	**Values**	**Units**
Diluter Physical (TPSG4/6)		
Max width	19.25 / 6.0	mm
Min height	30 / 30	mm
Max length	3000 / 3500	mm
Drift to septum	214 / 314	mm
Max septum Temp (Cu/H2O)	100 / 35	ºC
Beam		
Momentum	450	GeV/c
Time structure	25 ns bunches x 72 x 4	
Intensity	$1.1x10^{11}$ ($1.7x10^{11}$) $3.2x10^{13}$ ($4.9x10^{13}$)	Protons per bunch Total protons
Beam size at TPSG4 & TPSG6	σ_H 0.97 / 0.40 σ_V 0.63 / 0.58	mm mm

2. NUMERICAL ANALYSIS

The dynamic structural behaviour of the TPSG diluter blocks was studied by a numerical simulation tool developed at CRS4 which is based on the spectral element method (the ELSE code, see [6,7,8]). The study is focused on the interaction of the beam with the material and its possible consequences on the structural integrity of the target. The thermo-elastic problem is solved to estimate the temperature distribution, how stress waves propagate in the structure, and induced structural vibrations.

2.1 GEOMETRY

The TPSG4 and TPSG6 cores are 3.0 and 3.5 m long, respectively, and have the following material composition [9]: 2.4 / 2.6 m of graphite (CZ5/R6510, density 1.84 g/cm^3) + 0.3 / 0.3 m of titanium-aluminium alloy (TA6V, density 4.43 g/cm^3) + 0.3 / 0.6 m of nickel-based alloy (INCONEL 718, density 8.19 g/ cm^3).

Every material section is composed by a set of different parallelepipedal blocks. The dimensions of the blocks are: 30 mm (height) and 19.25 / 6.0 mm (thickness) for TPSG4 or TPSG6 respectively (Figure 5), several block lengths are adopted, in the rage between 10cm and 30cm.

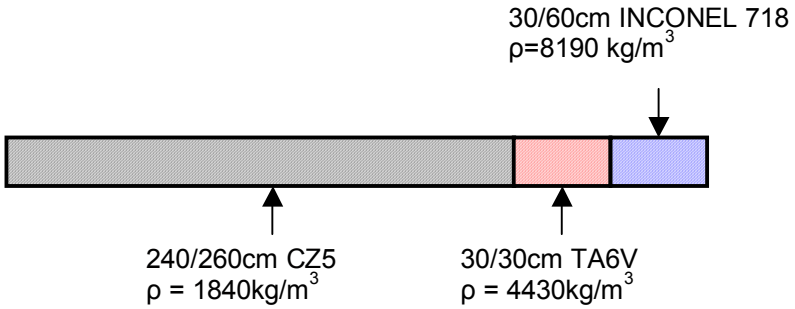

Figure 3 Dimensions and composition of TPSG4 & 6 diluter sections

2.2 MATERIAL PROPERTIES

The temperature-dependent thermal and mechanical properties of graphite CZ5 are shown in Figure 4, while values at room temperature (20°C) are listed in Table 2. Density and Poisson modulus are constant with temperature.

The properties at room temperature for the titanium alloy TA6V are listed in Table 3. Temperature-dependent values are presented in Figure 5.

The properties at room temperature for the INCONEL 718 alloy are listed in Table 4 while their trends with respect to temperature is shown in Figure 6.

Table 2 Graphite CZ5 properties at 20°C

Property	**Value**	**Units**
Density (ρ)	1840	kg m^{-3}
Specific heat (c_p)	685	J kg^{-1} K^{-1}
Thermal conductivity (k)	99	W m^{-1} K^{-1}
Thermal expansion coefficient (α)	3.92	10^{-6} K^{-1}
Elastic modulus (E)	11440	MPa
Poisson's ratio (ν)	0.15	-
Tensile strength (σ_t)	33	MPa
Compressive strength (σ_c)	125	MPa

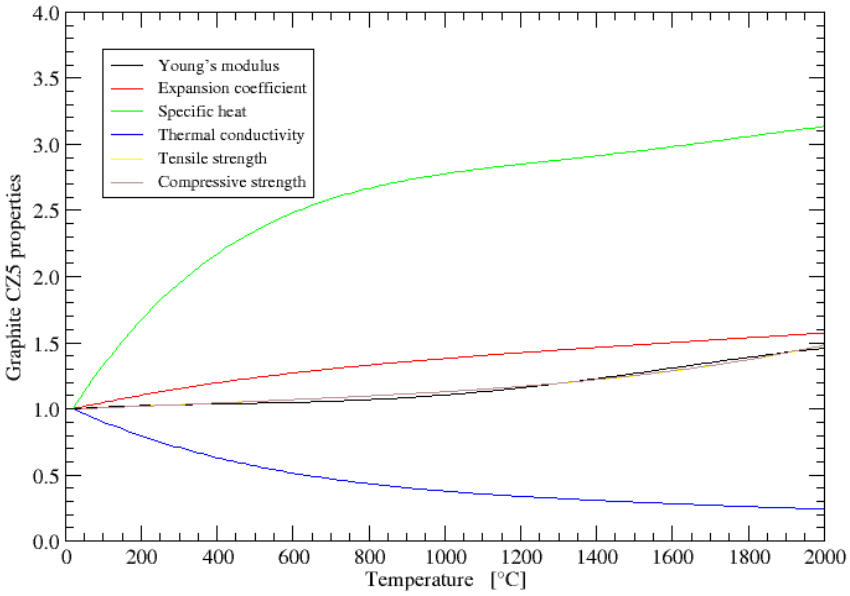

Figure 4 Graphite temperature-dependent properties, with respect to the values at room temperature (20° C), provided in Table 2

Table 3 Titanium alloy TA6V properties at 20°C

Property	**Value**	**Units**
Density (ρ)	4430	kg m^{-3}
Specific heat (c_p)	562	J kg^{-1} K^{-1}
Thermal conductivity (k)	6.62	W m^{-1} K^{-1}
Thermal expansion coefficient (α)	8.80	10^{-6} K^{-1}
Elastic modulus (E)	111900	MPa
Poisson's ratio (ν)	0.15	-
Tensile strength (σ_t)	1036	MPa
Compressive strength (σ_c)	1036	MPa

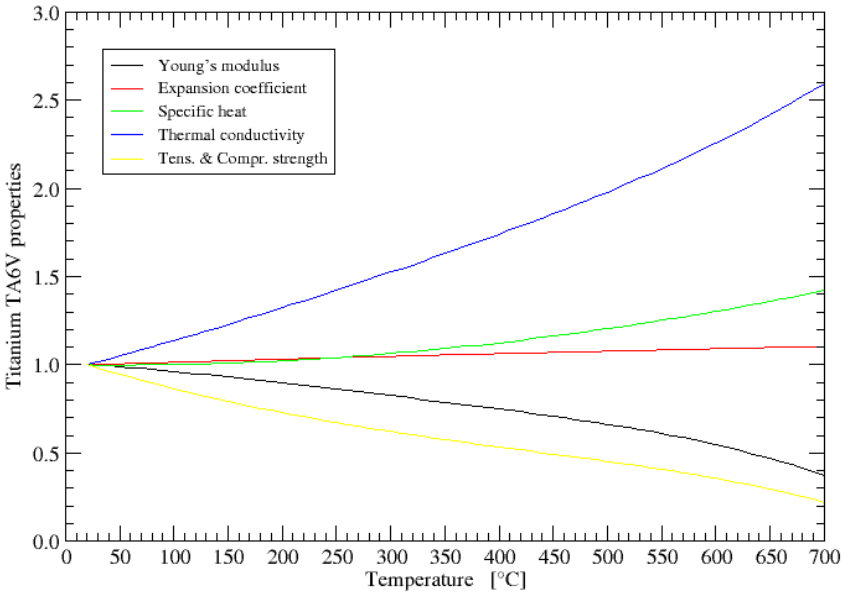

Figure 5 Titanium TA6V temperature-dependent properties, with respect to the values at room temperature (20° C), provided in Table 3

Table 4 INCONEL 718 properties at 20°C

Property	**Value**	**Units**
Density (ρ)	8190	kg m^{-3}
Specific heat (c_p)	437	J kg^{-1} K^{-1}
Thermal conductivity (k)	10.2	W m^{-1} K^{-1}
Thermal expansion coefficient (α)	12.80	10^{-6} K^{-1}
Elastic modulus (E)	207689	MPa
Poisson's ratio (ν)	0.284	-
Tensile strength (σ_t)	1408	MPa
Compressive strength (σ_c)	1408	MPa

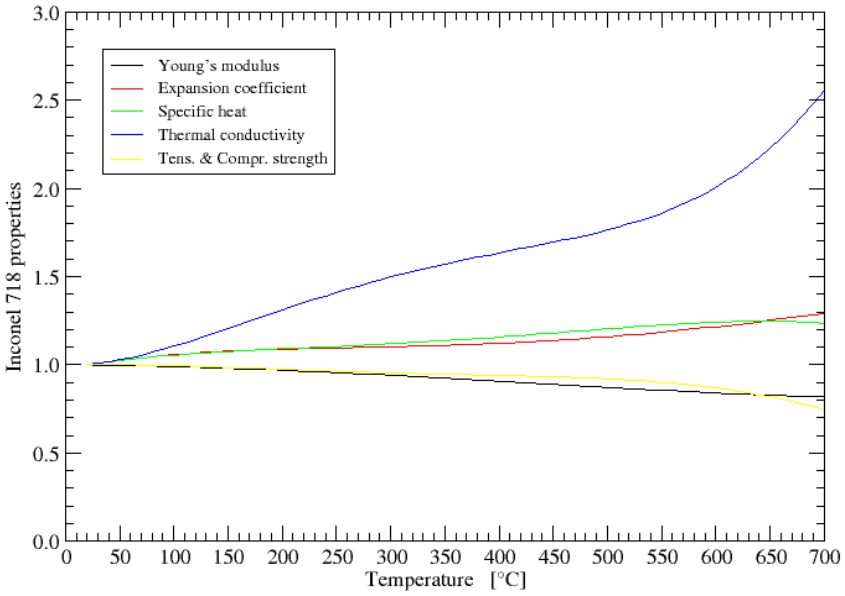

Figure 6 INCONEL 718 temperature-dependent properties, with respect to the values at room temperature (20° C), provided in Table 4

2.3 MODEL

The TPSG4 beam diluter is composed by ten graphite blocks 240mm long, plus two blocks 300mm long, whose materials are a titanium alloy (TA6V) for the first and INCONEL 718 for the second.

Each block is considered separately, the effect of the supporting structure being neglected. The mesh has been designed to fulfil the crucial requirement of accuracy, in particular in those parts, such as the block external surfaces where maximum stresses are expected. A second requirement was to maintain the numerical complexity of the model within reasonable limits. The spectral element mesh is shown in Figure 7 for the graphite block of TPSG4: it consists of 85000 spectral elements of variable dimensions ranging from 0.4mm to 10mm.

TPSG6 is composed by ten graphite blocks 250mm long, plus one 10cm graphite block, the titanium portion is formed by two 15cm long blocks, and the INCONEL final part is formed by a 10cm block followed by two blocks 25cm long.

Figure 8 shows the grid adopted for a 250mm long graphite TPSG6 diluter block, consisting in 27200 spectral elements.

The grid used for the other graphite, titanium and INCONEL blocks are perfectly similar to those here shown: the same section and element density is used, but the grid length is modified to be compliant to the block overall dimensions.

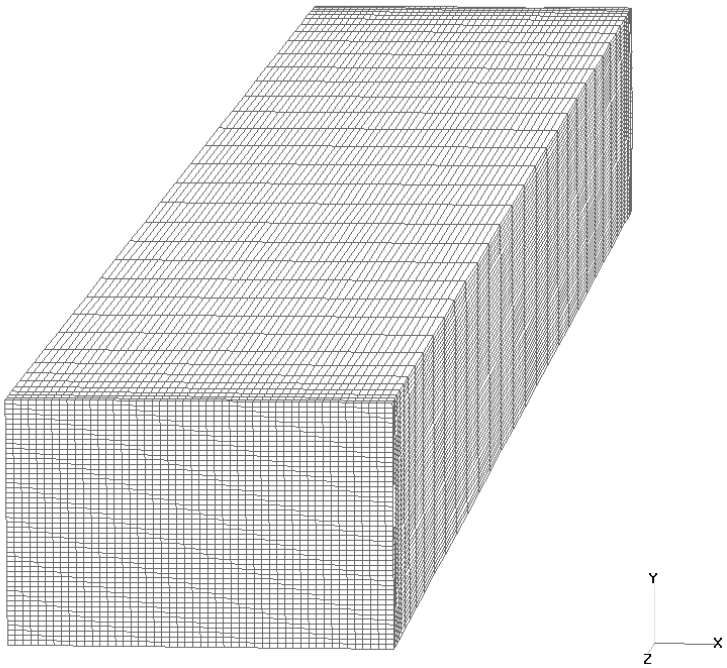

Figure 7 TPSG4 graphite block 3D grid

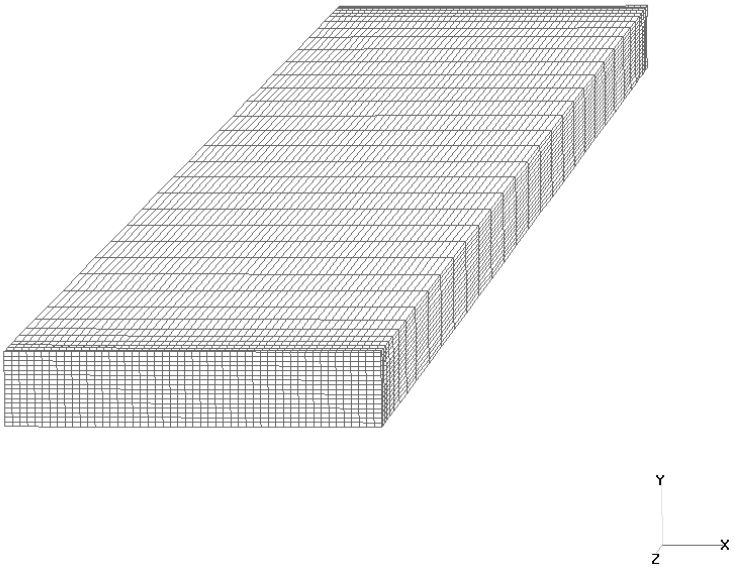

Figure 8 TPSG6 graphite block 3D grid

The spectral element formulation of the structural problem is based on the dynamic elasticity equation, coupled with the thermal equilibrium equation. The degrees of freedom of this problem are therefore the displacement components in the three directions and the temperature increase in each spectral node. A spectral degree

equal to 2 has been selected for the simulations, resulting in almost 3 million degrees of freedom for the TPSG4 graphite model.

2.4 LOAD

The load in the TPSG4 & TPSG6 have been calculated using the Monte Carlo FLUKA package version 2003 [10,11]. Non symmetrical (x,y,z) cartesian binning meshes with 100 vertical steps of $\Delta x = 0.03$ cm, 100/30 horizontal steps of $\Delta y = 0.02$ cm and 300/350 longitudinal steps of $\Delta z = 1.0$ cm were applied to score the density of energy deposited in the TPSG4/TPSG6 diluter element and in the subsequent MSE/MST copper septa.

The results of energy deposition on the TPSG4 show that the first meter of the graphite section is the most critical one: the local concentration of deposited energy reaches the maximum value of 0.24 ± 2.5% GeV/cm^3 per primary proton at about 16 cm depth in the graphite rod. Moreover, the longitudinal and radial gradient of energy deposition is steepest for the first 15 cm, thus the maximum temperatures and resultant thermal stresses are expected in this section, even though the total energy deposited in graphite amounts to only 25.5 GeV/p (i.e. 5.5% of the total incident proton energy). Similarly, the local concentration of deposited energy reaches a maximum value of 0.25 ± 3% GeV/cm^3 per primary proton at about 10 cm depth in the titanium block and 0.25 ± 6% GeV/cm^3 per primary proton at about 2 cm depth in the INCONEL block. 160 GeV/p are deposited in the yoke of the diluter element (36%), and the rest of the energy (54.9%) is deposited outside by particles escaping the system.

2.5 BOUNDARY CONDITIONS AND ASSUMPTIONS

Individual analyses were run for each block, whose external surfaces and extremities are assumed to be free with an initial temperature of 20ºC. The effect of the support system is therefore neglected: elastic waves are fully reflected at these free boundaries, so that their energy is confined in the block.

Convection, radiation and conduction are not included. The thermal problem is entirely governed by the heat capacity of the material.

2.6 FAILURE CRITERIA

The severity of the thermal load on the TPSG was estimated by comparing pointwise the computed stress at a given time with a reference failure limit. In this study, the Stassi limit criterion has been adopted for isotropic graphite, titanium and INCONEL. Titanium and INCONEL alloys are characterized by the same value of strength in tension and in compression, the Stassi criterion reduces to the Von Mises criterion.

The Stassi criterion may be figured out as a generalized version of the classic Von Mises stress criterion which takes into account the effects of pressure and the difference (if any) between the tensile and compressive strength of a material.

The tensile equivalent Stassi stress σ_{teq} is calculated from the following equation

$$k\sigma_{teq}^2 + 3(k-1)p\sigma_{teq} - \sigma_{vm}^2 = 0$$

where k is the ratio between compressive and tensile strength, σ_{vm} is the Von Mises equivalent stress and p is the internal pressure

$$k = \sigma_c / \sigma_t \qquad p = -\tfrac{1}{3}(\sigma_1 + \sigma_2 + \sigma_3)$$

where σ_1, σ_2, and σ_3 are the principal stresses.

In the following, we make use of the Stassi stress ratio:

$$\varepsilon_{St} = \sigma_{teq} / \sigma_t$$

This ratio corresponds to the reciprocal of the commonly used safety factor: it has a low value where stress is low, and increases from zero to unity as failure is approached. Values higher than unity imply the rupture of the material.

3. TPSG4 RESULTS

In the particle interaction analysis provided by FLUKA the beam has been focused on the centre of one of the pipes of the MSE coil, and it is therefore not centred on the TPSG4 blocks. All the 12 diluter blocks have been analysed separately for a minimum duration of 250μs, sufficient to evaluate several wave reflections inside the blocks.

In the graph of Figure 9 the maximum temperature increase in each of the diluter blocks is shown. The maximum value is reached in the 2nd graphite block where the energy is highly focused around the beam axis and then rapidly decreases along the diluter length, where energy power deposition is lower and/or less concentrated.

Temperature increase is high also for the titanium and INCONEL blocks, due to their different material properties.

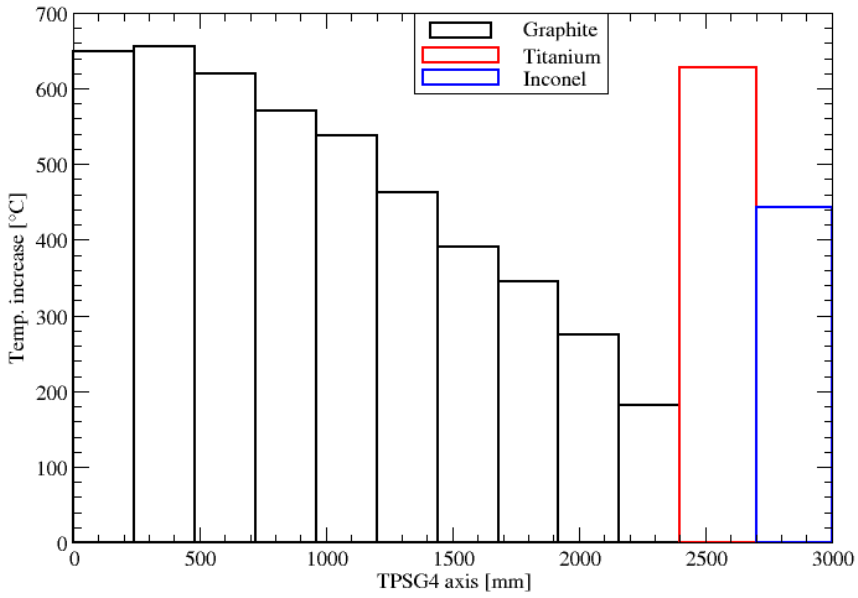

Figure 9 Maximum temperature increase in TPSG4 diluter blocks

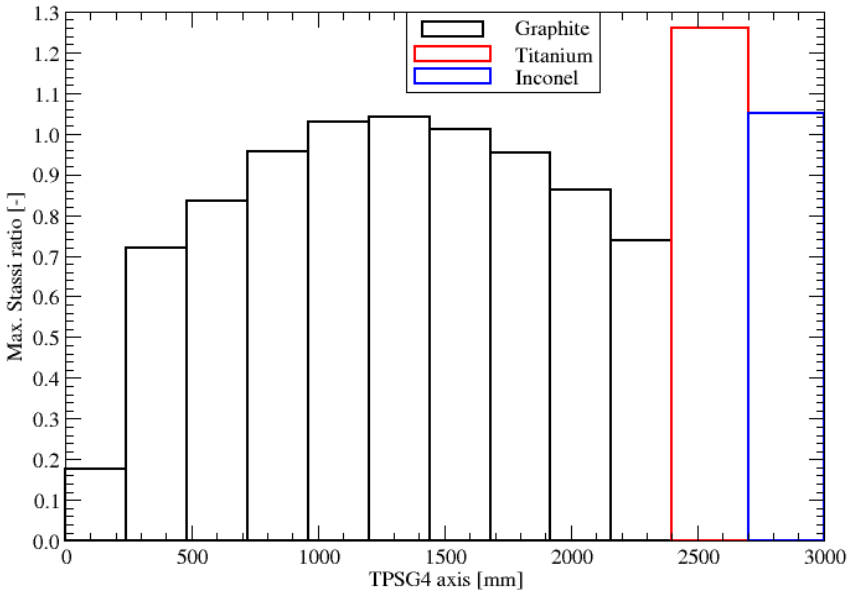

Figure 10 Maximum Stassi ratio for a 250μs simulation in TPSG4 diluter blocks

Figure 10 shows the maximum value of the Stassi stress ratio. The graph summarises the result of the simulations run for each of the diluter blocks: for each block the maximum value of the Stassi ratio in any point of the block and at any time during a 250 μs simulation is taken.

The stress level is very high (we recall that with Stassi ratio we mean the ratio between the Stassi tensile equivalent stress and the tensile rupture strength of the material).

3.1 GRAPHITE

Looking at the results in Figure 9 and Figure 10 for the graphite blocks, it can be verified that the highest stresses are not found on the same block for which the maximum temperature increase was reached. The 6th block results to be the most stressed.

The plots of Figure 11 and Figure 12 show the temperature increase in the 2nd and 6th absorber block. Temperature increase is directly related to the power deposition in the blocks; it is clear that the power deposition is more focused around the beam axis for the 2nd block with respect to the 6th block, where an increase in temperature in a wider area is visible.

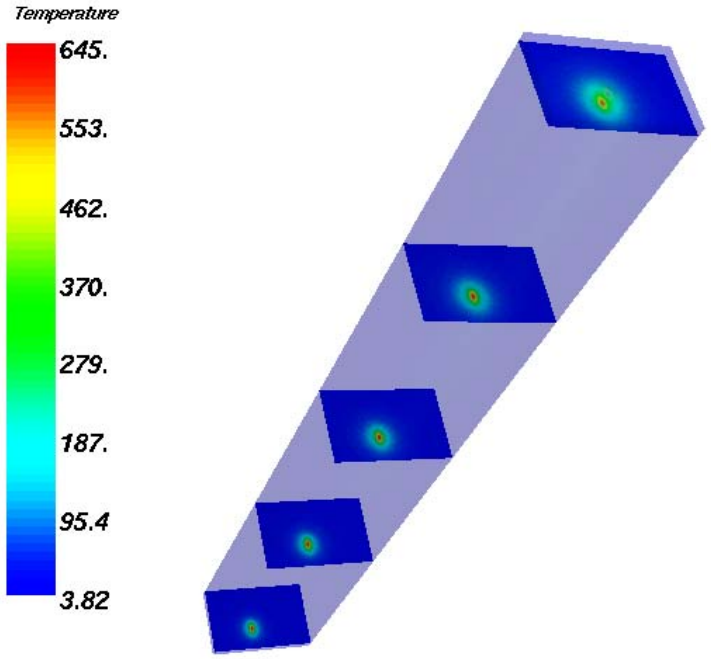

Figure 11 Temperature increase [°C] for the 2nd graphite diluter block

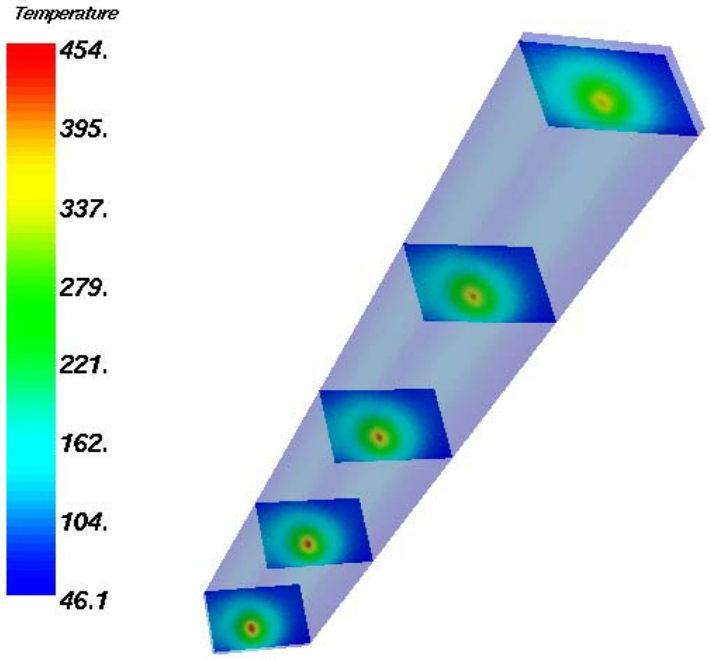

Figure 12 Temperature increase [°C] for the 6th graphite diluter block

Stresses in the blocks are related to the temperature increase value and to the steepness of the radial distribution of temperature: the higher the temperature and the steepness, the higher the stresses.

Anyhow, stress intensity is related also to the beam axis position with respect to the external surface of the block: previous studies have shown that is possible to

find critical distance of the beam axis from a block surface that maximizes the resulting stress intensity [7]. This distance was found to be slightly greater than the mean radius of the energy distribution in given section.

In the TPSG4 diluter as the power density radial distribution becomes less steep moving from the 1st to the 10th block, there is a block (the 6th) for which the balance between the temperature increase and the critical distance of the beam axis from a block surface reaches a maximum.

The Maximum Stassi ratio distribution during the simulation is shown in Figure 13 for the 2nd block and in Figure 14 for the 6th block.

In both cases the most stressed points are located on the external surfaces of the block where reflection of radial stress waves occurs.

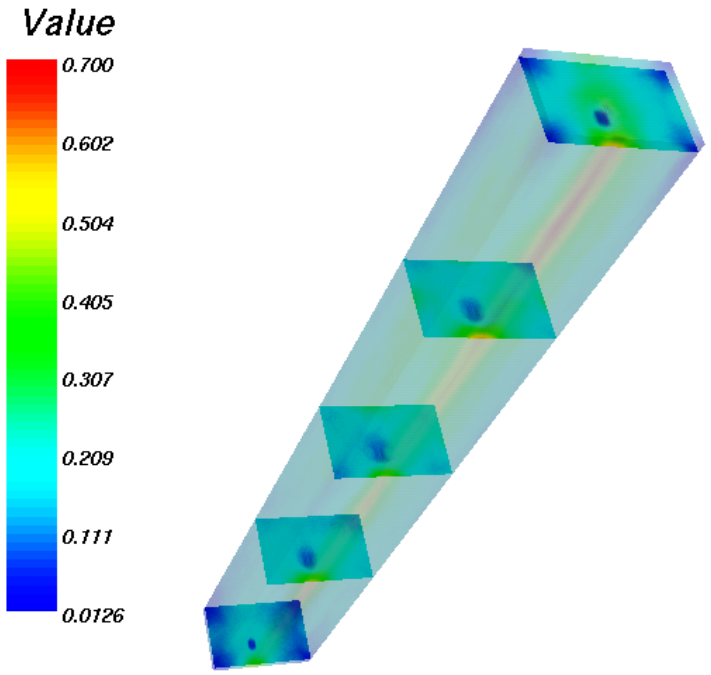

Figure 13 Maximum Stassi ratio [-] in the 250μs simulation for the 2nd graphite diluter block

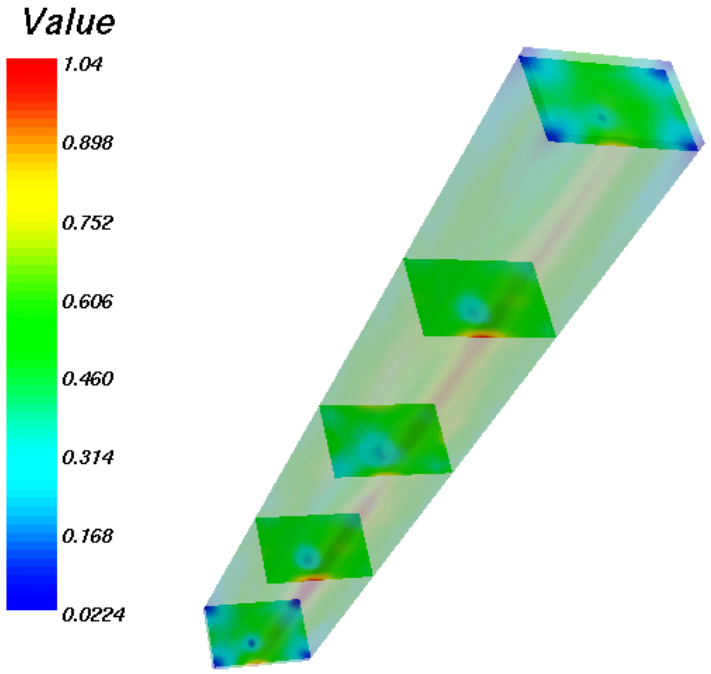

Figure 14 Maximum Stassi ratio [-] in the 250μs simulation for the 6th graphite diluter block

Figure 15 shows the Stassi ratio color plot on the 2nd block at different times. Both longitudinal and radial stress waves propagate in the block, and their superposition let the stress pattern difficult to be distinguished.

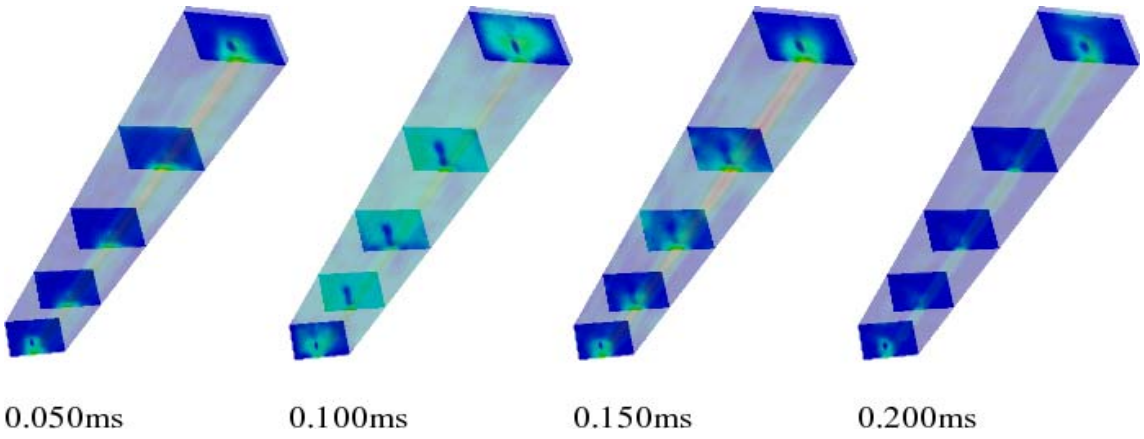

Figure 15 Stassi ratio [-] for the 2nd graphite diluter block at different times during the 250μs simulation

As mentioned before, the higher value of the maximum Stassi stress ratio on the 6th block is partly caused by the wider section on which the beam power is deposited.

We present here the results of two simulations on the 2nd block (where the maximum power density is deposited): the beam axis is moved towards the external surfaces along the y direction.

Figure 16 and Figure 17 show the temperature distribution and the maximum Stassi ratio value on 2nd graphite block when the beam axis is located 2.28mm from

the lateral surface. The distance is approximately equal to $1.167\sigma_y$, being σ_y the mean radius of the energy distribution profile along the y direction.

Temperature increase is more or less equal to the previous results, and higher stresses are found, as expected.

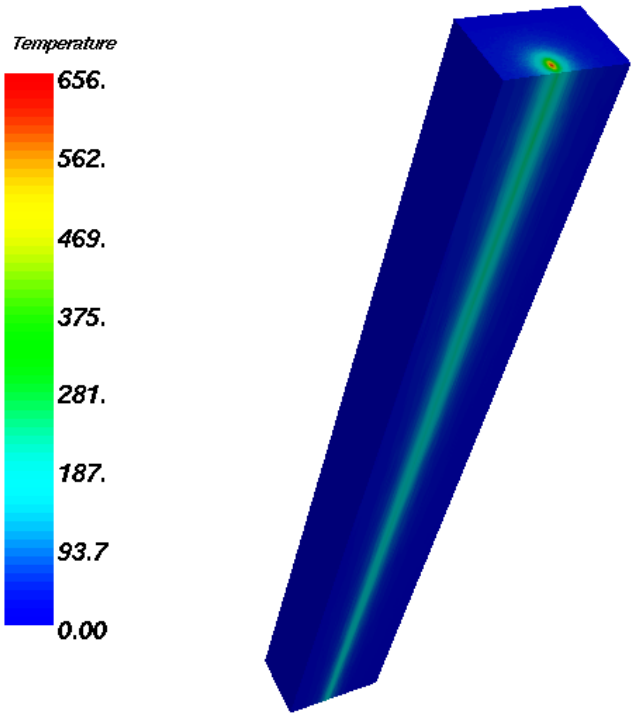

Figure 16 Temperature increase [ºC] for the 2nd graphite diluter block when the beam axis is 2.28 mm distant from the lateral surface

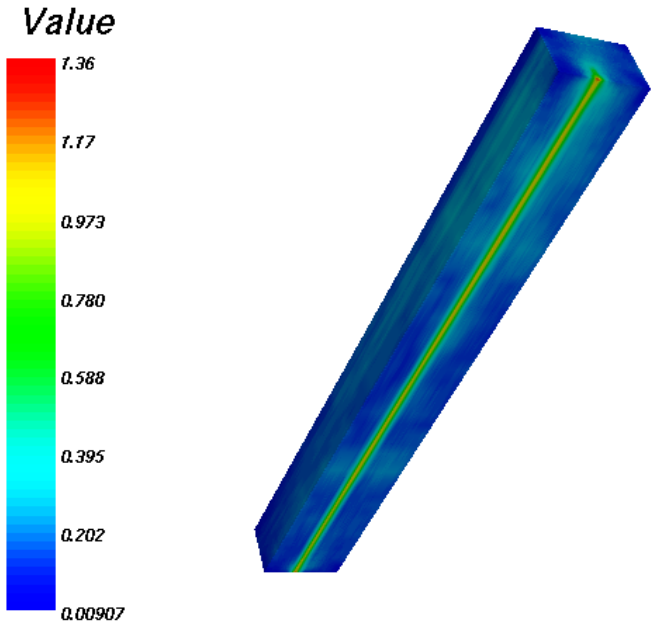

Figure 17 Maximum Stassi ratio [-] in the 250μs simulation for the 2nd graphite diluter block when the beam axis is 2.28 mm distant from the lateral surface

Moving the beam focus point to this new position gives rise to values higher than unity for the maximum Stassi ratio: rupture would occur with these load conditions.

3.2 TITANIUM

Immediately after the 2.4m long graphite part of the TPSG4, there is a 30cm long block made of a titanium base alloy TA6V. The cross section of this block is the same as for the graphite blocks, while the length is different, as well as the position along the beam axis. The power deposition in this block is characterized by a wider cross section; moreover the different material causes and higher value of the power density.

Figure 18 shows the temperature increase in the titanium TPSG4 diluter block in a section that includes the beam axis. The temperature increase caused by power deposition is higher than the temperature in the last graphite blocks before the titanium.

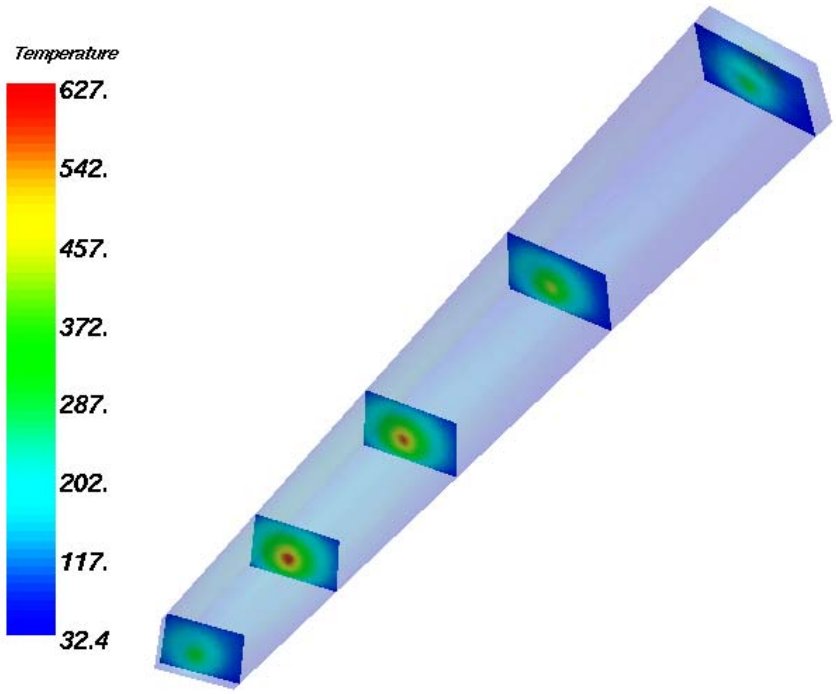

Figure 18 Temperature increase [ºC] in the TA6V TPSG4 diluter block

Figure 19 and Figure 20 show the maximum Stassi ratio value found in each point of the block during the 250μs long simulation. The most severe stress conditions are found on the external surface closer to the beam axis near the region of maximum density of power deposition.

The results show that the maximum Stassi ratio found during the simulation is higher than unity, meaning that at least in one instant the Stassi equivalent stress results higher (of a factor 1.28) than the rupture stress of the material. The design cannot therefore be considered safe for this load condition.

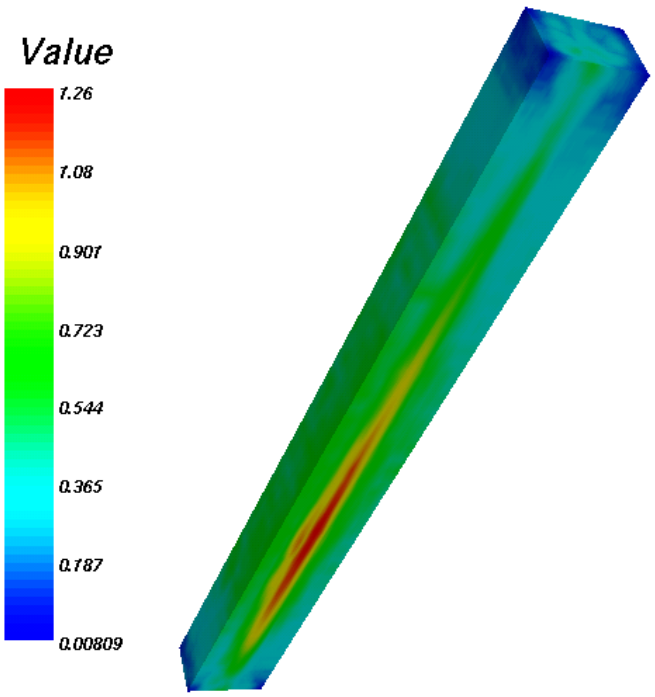

Figure 19 Maximum Stassi stress ratio [-] in the TA6V TPSG4 diluter block, for a 250µs long simulation

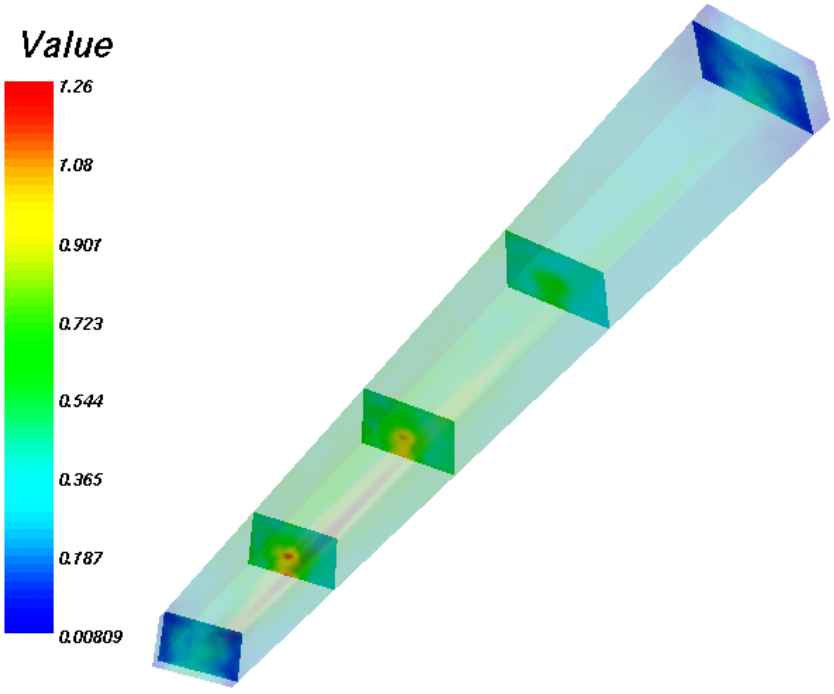

Figure 20 Maximum Stassi stress ratio [-] in the TA6V TPSG4 diluter block, for a 250µs long simulation

As for the graphite blocks we look for a different positioning of the beam, that should maximize the resulting maximum Stassi ratio on the titanium block.

The beam is moved towards the lateral surface, setting the beam axis 10.8mm far from the surface. The value of the beam distance is proportional to the mean radius of beam power distribution in the radial direction, for the section of maximum power deposition on this block.

The temperature distribution is not expected to depend from the different beam focus position; on the other hand, the stresses should increase with respect to the initial configuration.

Figure 21 shows the temperature increase distribution on the diluter block when the beam is moved closer to the lateral surface. The results are pretty similar to those previously found. A minor problem in the FLUKA file is that this grid exactly covers the titanium block dimensions; forcing a misalignment between the spectral element and the Monte Carlo grids, some part of the structural grid would not feature the exact value of the power deposition. To get a more precise result a new FLUKA analysis would be performed.

Figure 22 shows the maximum Stassi ratio found in the block during the simulations. This time there is not much difference between the stress results when the beam is in the initial position and when is closer to the surface: this may be related to the fact that the power deposition area is very spread over the titanium block. The maximum value of the Stassi ratio is anyway well over unity, thus suggesting an high probability of failure in the material for these load conditions.

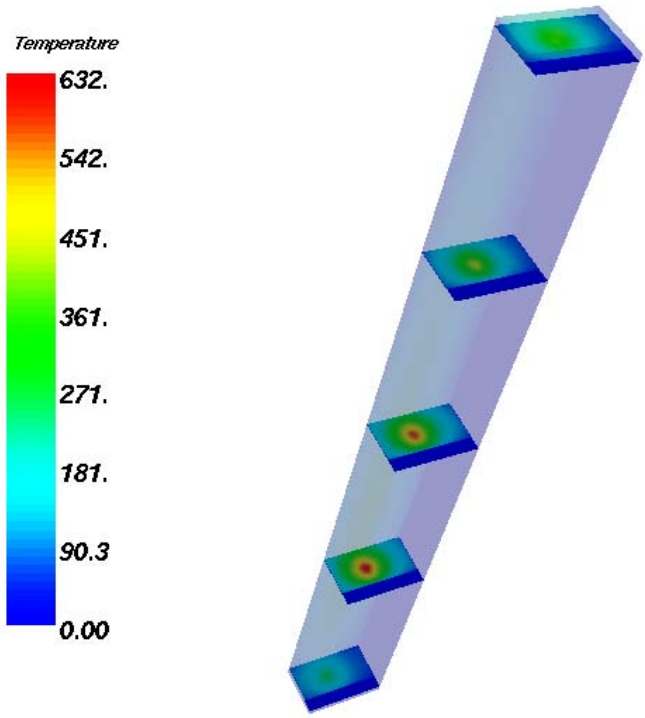

Figure 21 Temperature increase [ºC] for the TA6V diluter block when the beam axis is 10.8mm distant from the lateral surface

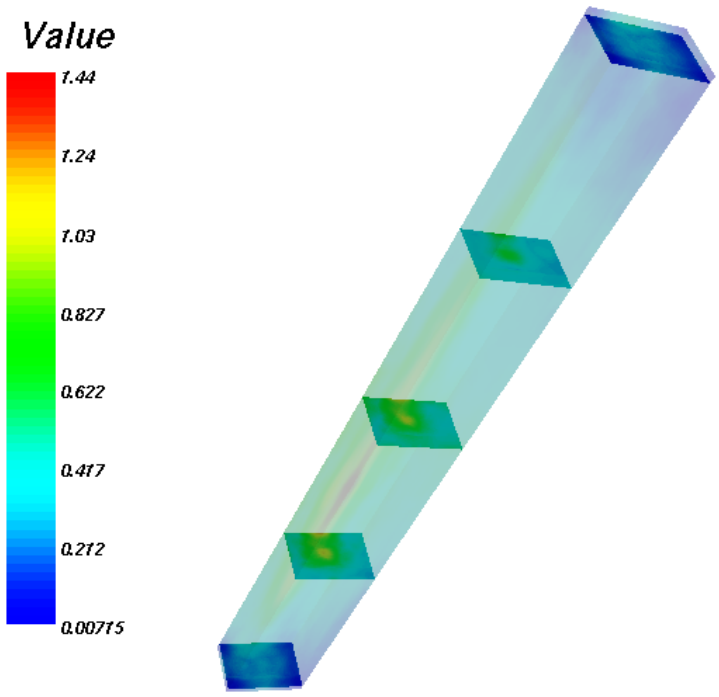

Figure 22 Maximum Stassi ratio [-] in the 250μs simulation for the TA6V diluter block when the beam axis is 10.8mm distant from the lateral surface

3.3 INCONEL 718

The last diluter block of the TPSG4 is made of INCONEL 718 alloy. The external dimensions of this block are the same of the titanium block, located immediately before the INCONEL following the beam trajectory. Since this block is located at the end of the diluter, the power deposition section area is the widest of all the blocks. The nuclear and thermal properties of this material are different from the previous and higher power deposition intensity and/or higher temperature increase may be recorded in this block.

Figure 23 shows the temperature increase in the INCONEL 718 block; the power deposition is highly concentrated in the first part of the block, where the temperature increase is quite high, with a maximum value of 443ºC in the beam axis.

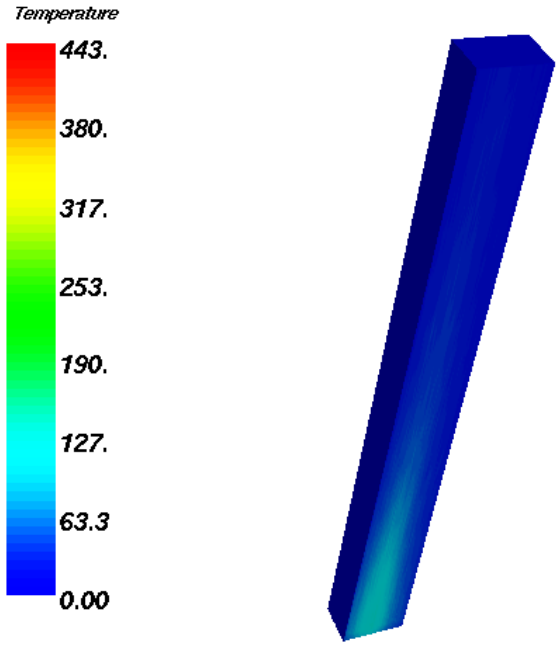

Figure 23 Temperature increase [ºC] in the INCONEL 718 TPSG4 diluter block

Figure 24 shows the maximum Stassi ratio value found in each point of the block during the 250μs long simulation. The most severe stress conditions are on the external surface closer to the beam axis near the region of maximum density of power deposition, near the first end of the block. In these points the maximum Stassi ratio results to be higher than unity (1.05) at least once during the simulation meaning that in those points the Stassi tensile equivalent stress has become larger than the tensile failure value, even if by a small factor.

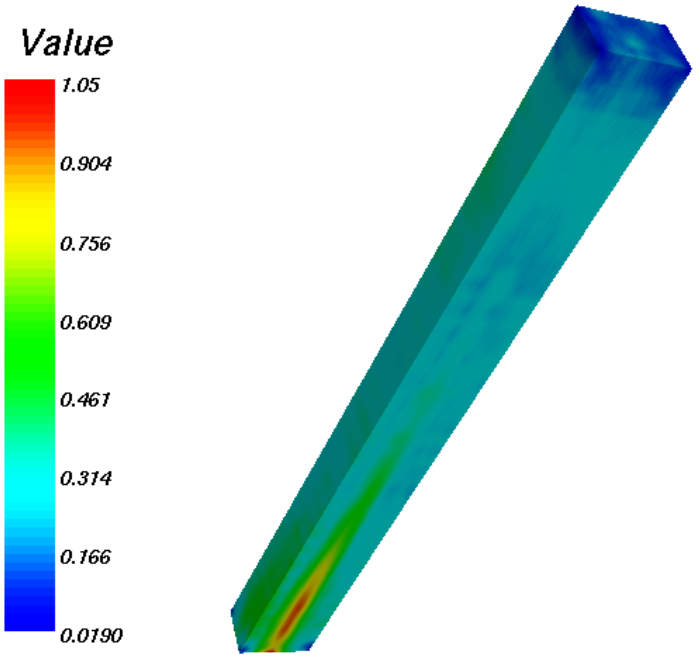

Figure 24 Maximum Stassi stress ratio [-] in the INCONEL 718 TPSG4 diluter block, for a 250μs long simulation

4. TPSG6 RESULTS

Each of the 16 blocks of the TPSG6 diluter has been analysed separately with 250μs long simulations: this, again, should allow to have a complete view of the structural behaviour of this equipment when subject to the particle beam power deposition and heating.

The graph in Figure 25 shows the maximum temperature increase in each of the diluter blocks of the TPSG6.

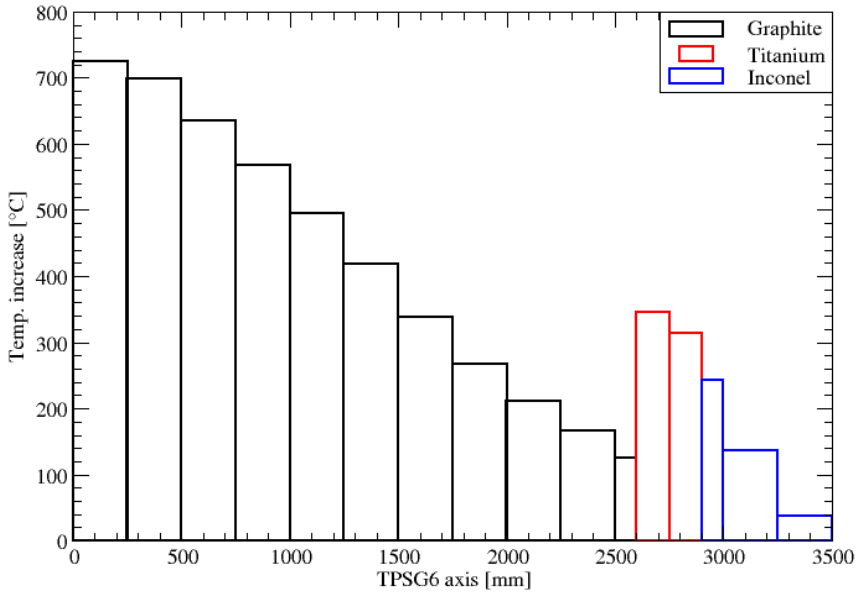

Figure 25 Maximum temperature increase in TPSG6 diluter blocks

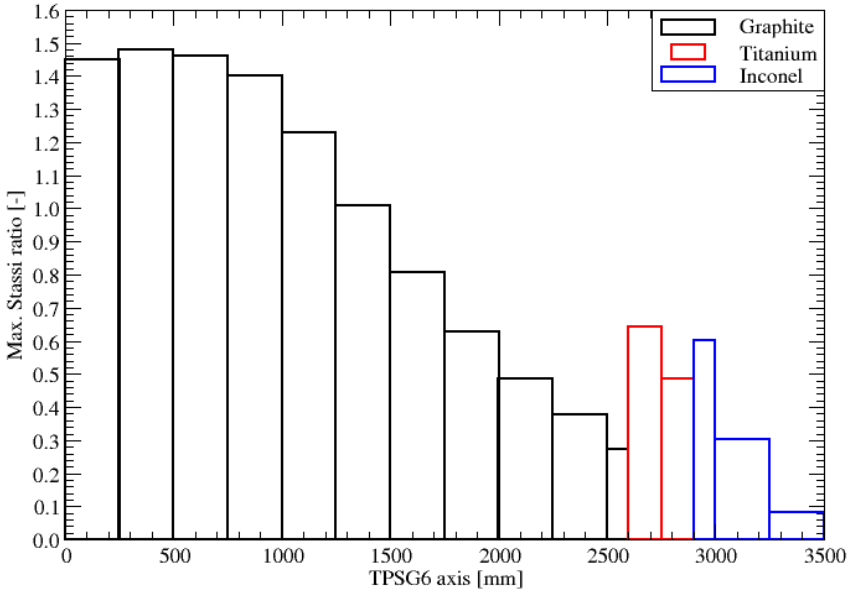

Figure 26 Maximum Stassi ratio for a 250μs simulation in TPSG6 diluter blocks

The maximum temperature increase this time is reached in the 1st graphite block, where the beam is highly focused around the axis and the energy density is very high. The power density around the beam axis and the maximum temperature reached in the block decreases along the beam axis and the target length.

The maximum value of the Strassi ratio found in any point of each graphite block in a 250μs long simulation is shown in Figure 26. Stress values are high and

even higher than those found for the TPSG4 diluter. This is probably due to the different cross section of the TPSG6: the block faces are closer to the beam axis and therefore the effect of the proximity of the beam to a lateral surface is relevant.

The most critical block turns out to be the 3rd where a value of almost 1.5 is reached. This means that during the simulation at least in one point of this block the ratio between the Stassi tensile equivalent stress is 1.5 higher than the graphite tensile rupture stress; a damage of the material is highly probable.

4.1 GRAPHITE

Figure 27 shows the temperature increase due to the beam power deposition in the 2nd block. This block is close to the beginning of the diluter and the beam powered is still well focused around the beam axis; temperature increase is clearly proportional to the deposited energy.

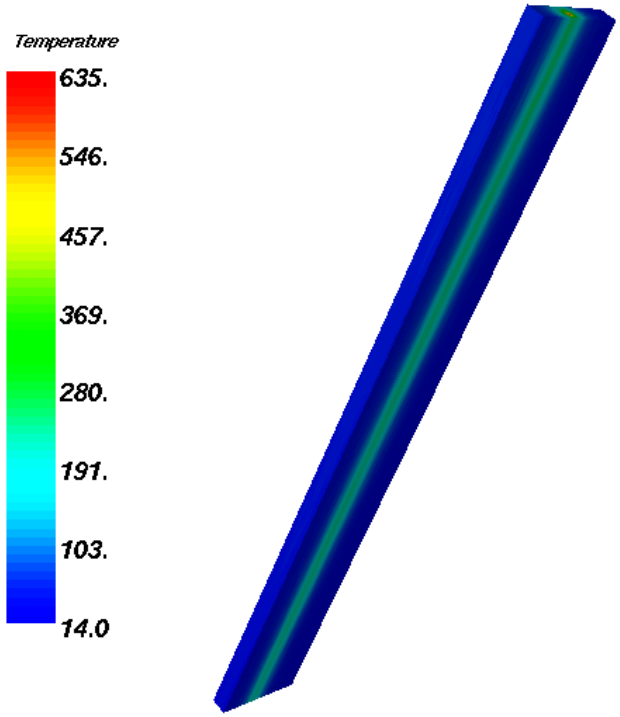

Figure 27 Temperature increase [°C] for the 2nd graphite diluter block

The 2nd block is not the one featuring the highest temperature increase, as visible in the graph of Figure 25, even if the maximum temperature increase is still quite high. It is indeed the block where the highest stresses take place, even if (see Figure 26), similar values are reached in the 1st and in the 3rd block too. Stress intensity is obviously related to the temperature increase, but also to the steepness of the radial temperature profile and to the beam axis position in the block.

The maximum value of the Stassi ratio found in each point of the 2nd block during the simulation is shown in the color plot of Figure 28; the most stressed points are on the external surfaces, near the beam axis and near the block end surfaces in particular. The maximum stress ratio is significantly higher than unity, corresponding to material rupture: this high value is limited to a small portion of the TPSG6 block. Nevertheless, relevant stresses are present in a large portion of the block with values close to unity near the beam axis.

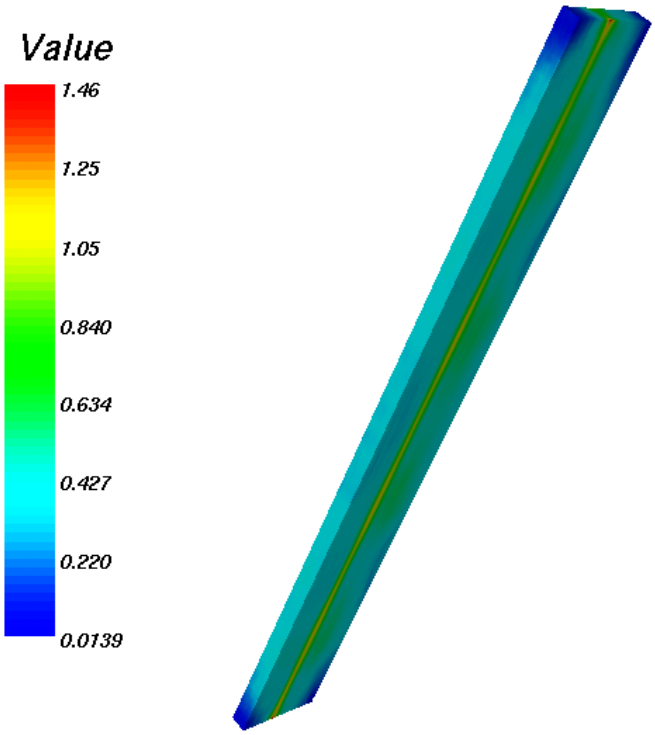

Figure 28 Maximum Stassi ratio [-] in the 250μs simulation for the 2nd graphite diluter block

4.2 TITANIUM

Following the beam trajectory, the nearest neighbour of the graphite portion of the TPSG6 diluter are two 15cm long blocks made of TA6V, a titanium base alloy.

The cross section of these blocks is the same of the graphite blocks; the power deposition is characterized by a wider cross section, due to the effect of the previous blocks and to the different nuclear properties of the material.

The results in Figure 25 and Figure 26 show that the 1st block has higher values of temperature increase and maximum stress level achieved in the simulation.

Figure 29 shows the temperature increase distribution for the 1st titanium block. The highest values are found near the first block end, with values higher than those found on the last graphite blocks, due to the different nuclear and thermal properties of the material.

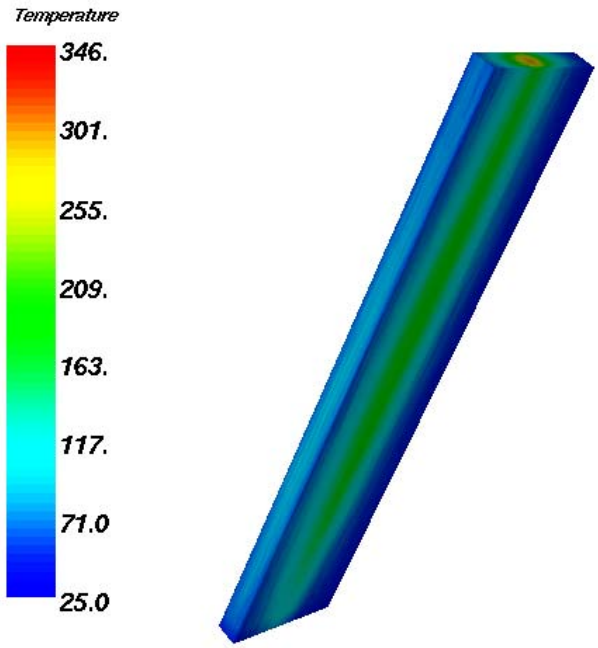

Figure 29 Temperature increase [ºC] in the 1st TA6V TPSG6 diluter block

Figure 30 show the maximum Stassi ratio value found in each point of TA6V block during the 250μs long simulation. The most severe stress conditions are on the external surface closer to the beam axis near the region of maximum density of power deposition and temperature increase. The stress distribution seems to be due mainly to the static stresses since the maximum values are found near the beam power deposition area; anyway, stress waves are present and are responsible of the approximately constant stress level found in the rest of the block.

The maximum value of the Stassi ratio is lower than unity, meaning that the stress level should not lead to a material failure under these load conditions: the ratio of the Stassi equivalent tensile stress with the tensile rupture stress during the simulation has reached (at least in one point) the maximum value of 0.64, that corresponds to a safety factor of 1.55 against rupture.

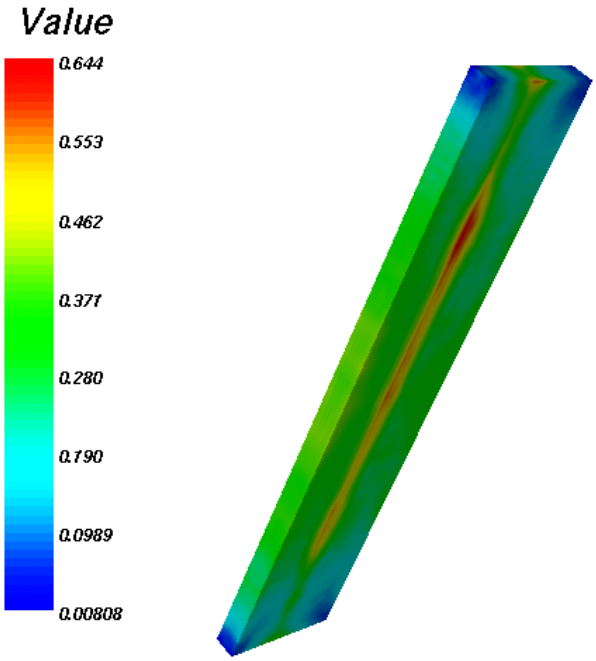

Figure 30 Maximum Stassi stress ratio [-] in the 1st TA6V TPSG6 diluter block, for a 250μs long simulation

4.3 INCONEL 718

The last portion of the TPSG6 diluter is made of the INCONEL 718 alloy: it consists in 3 blocks, the 1st 10cm long and the other two 25cm long; the cross section is the same adopted in the rest of the diluter.

The nuclear properties of the material are different from those of previous blocks; the beam power is spread over a wider cross section and is higher on the first sections of the block. The power deposition decreases rapidly along the INCONEL portion, and the maximum temperature and stresses are reached in the 1st block.

The temperature increase follows as usual the deposited beam power distribution and is shown in Figure 31 for the 1st block. Maximum values are found on the beam axis, and are quite low if compared to those found in the graphite blocks or in the TPSG4 block made of the same material.

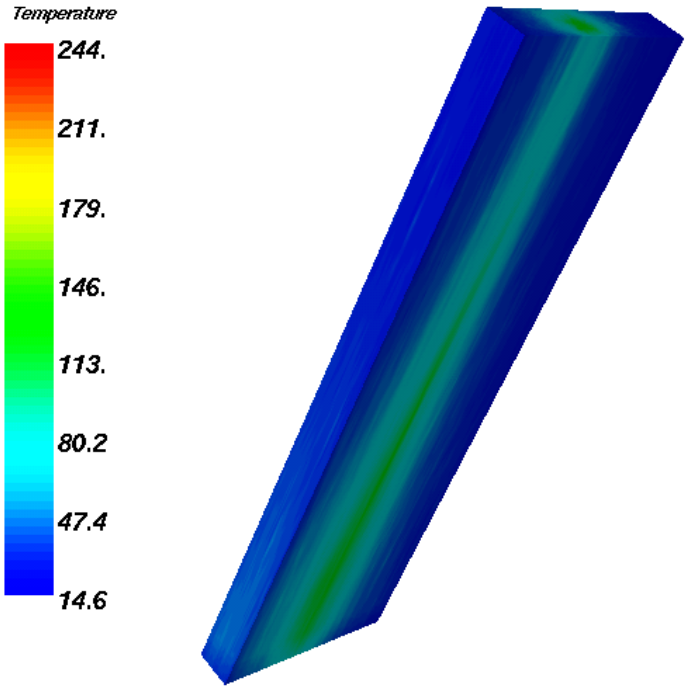

Figure 31 Temperature increase [ºC] in the 1st INCONEL 718 TPSG6 diluter block

The maximum Stassi ratio for each point of the 1st block during the simulation is shown in Figure 32: it is approximately constant for a large portion of the block, but higher values are found near the beam axis, where the maximum energy is deposited. Dynamic stress waves are responsible for the stress levels in all the block volume, but in the points near the beam axis where the maximum temperature increase is recorded, the static component of the stress sums to give the maximum value.

The most stressed point faces an equivalent tensile stress that is approximately the 60% of the tensile rupture value: this corresponds to a safety factor of 1.66 against rupture, suggesting that the INCONEL block may be considered safe under this load condition.

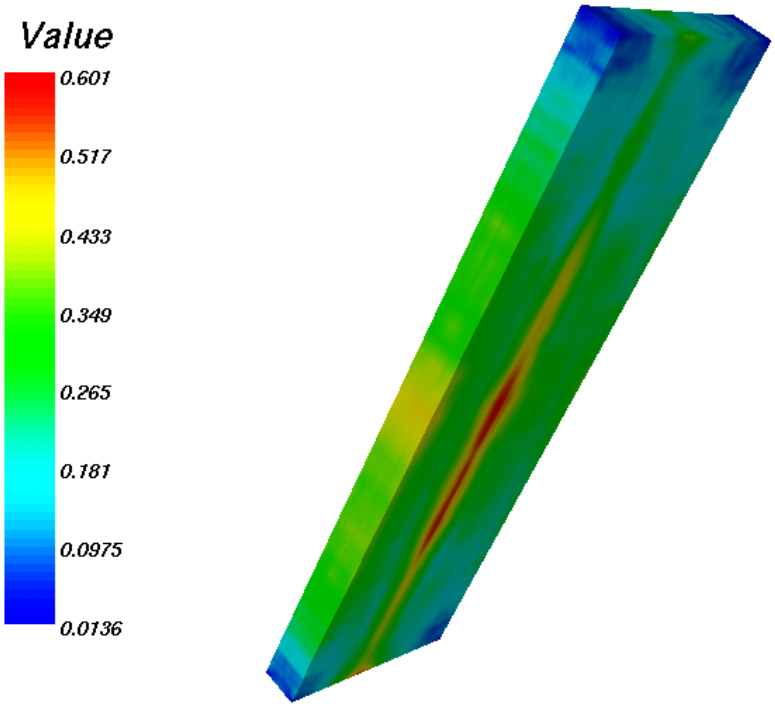

Figure 32 Maximum Stassi stress ratio [-] in the 1st INCONEL 718 TPSG6 diluter block, for a 250μs long simulation

5. LONG TERM BEHAVIOUR

All the results shown so far are obtained with numerical simulations on very detailed models, with a simulation length limited to the time required to capture the stress waves travelling in the structures after the beam heating.

This time length is normally sufficient to deal with the most important stress causes in structures like these, subject to this kind of load.

Anyway when the beam is not centred on the blocks, also transverse bending vibrations may be excited. Longer simulations are required to put in evidence these phenomena and coarser models are adopted in these simulations to keep computer time requirements within reasonable limits.

It is worth here to remind that no damping is adopted in these models, for the sake of simplicity and safety, and that material and structural damping may influence the long term structure behaviour in the real world.

In the following the results of the long term simulations for the most stressed graphite blocks of the TPSG4 and TPSG6 will be quickly described; it will turn out that the maximum resulting stresses are analogous to those already shown.

5.1 TPSG4

The 6th block has been analysed for a total time of 1.5ms, with the same loading conditions but using a coarser mesh. The block is considered free: no boundary conditions are applied on the displacements.

Figure 33 displays the three components of the displacements at one end of the block: the displacement along the z axis is essentially due to the longitudinal vibration of the block, the displacements along the x and y axes result from the

superposition of transverse and bending vibrations of the block, with bending vibrations having a lower frequency.

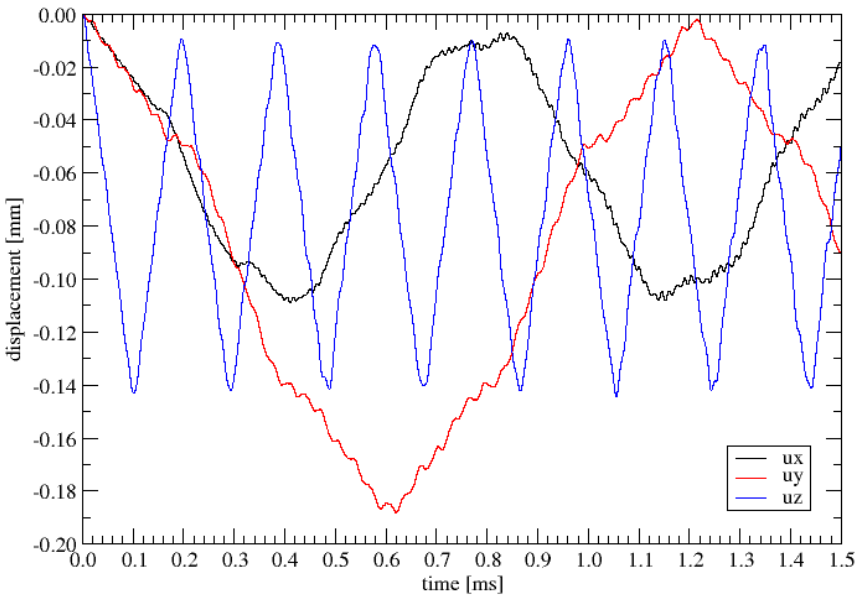

Figure 33 Displacements at an end of the 6th TPSG4 graphite block

The maximum value of the Stassi stress ratio found in each point of the block during the simulation is shown in Figure 34. The result is very similar to the one shown in Figure 14 for a shorter time length. The small difference in the maximum value should be due to the different model adopted.

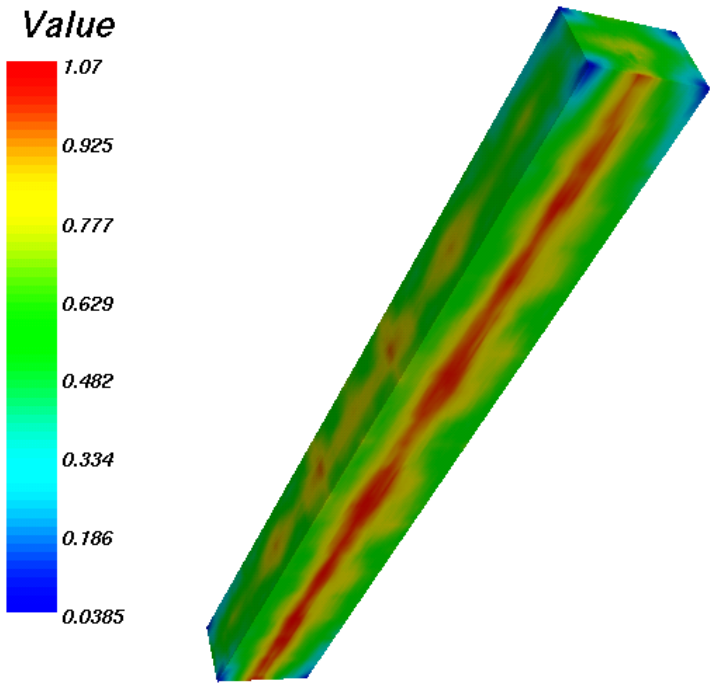

Figure 34 Maximum Stassi stress ratio [-] in the 6th TPSG4 graphite diluter block, for a 1.5ms long simulation

5.2 TPSG6

For the TPSG6 the attention is focused on the 2nd block. Since the structure is less rigid with respect to the TPSG4 blocks, the simulation length is set to 5ms. The loading and boundary conditions are the same adopted for the 250μs simulation, while a coarser model is used.

Figure 35 displays the three components of the displacements at one end of the block. The displacement along the z axis is essentially due to the longitudinal vibration of the block, the displacements along the x and y axes result from the superposition of transverse and bending vibrations of the block, with bending vibrations having a lower frequency. The block has a low stiffness for bending in the yz plane, therefore the displacement amplitude results high.

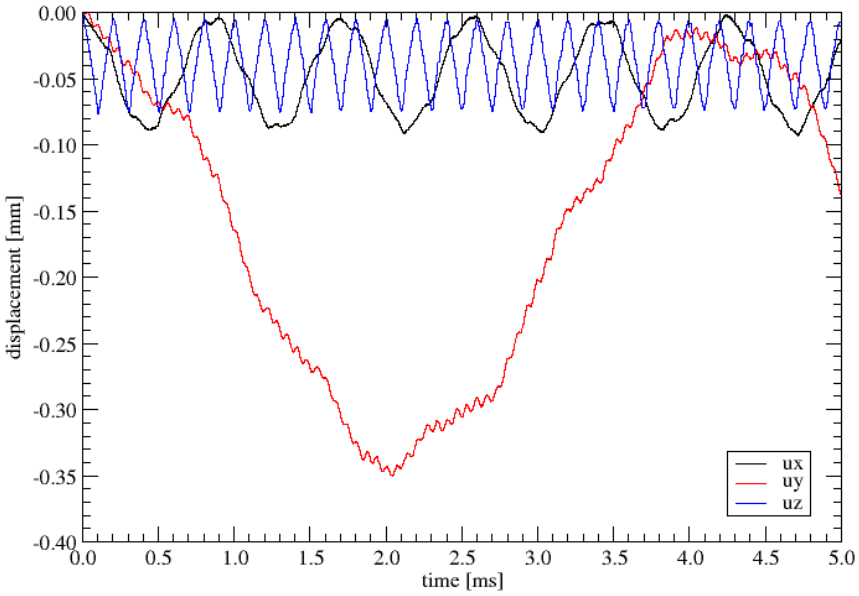

Figure 35 Displacements at an end of the 2nd TPSG6 graphite block

Figure 36 shows he maximum value of the Stassi ratio found in each point of the block during the simulation. The result is similar to that shown in Figure 28, and the higher value of the maximum should be related to the coarser mesh adopted.

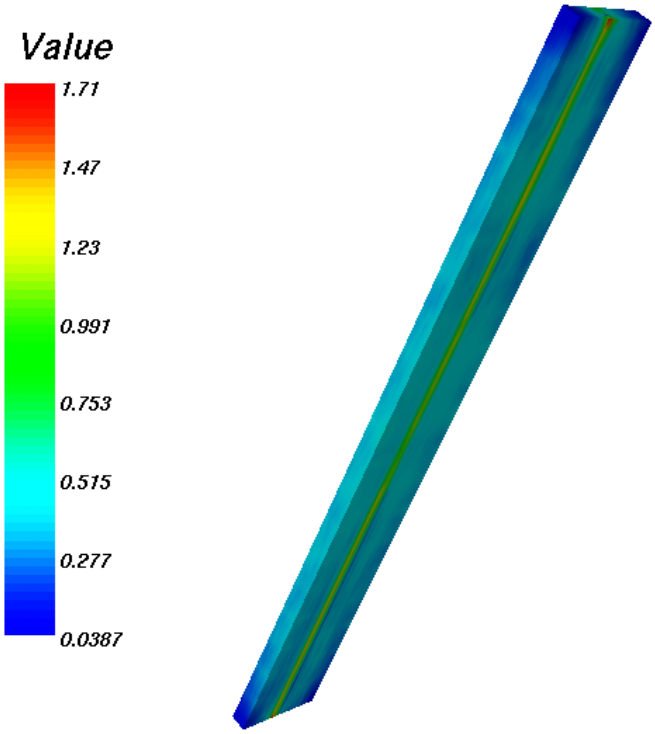

Figure 36 Maximum Stassi stress ratio [-] in the 2nd TPSG6 graphite diluter block, for a 5.0ms long simulation

6. CONCLUSIONS

A structural analysis of the TPSG4 and TPSG6 diluters was performed to verify their behaviour under the thermal load due to a fast extracted proton beam hitting.

The deposited energies are estimated by the particle transport code FLUKA and converted to internal heat generation rates according to the time dependence of the extracted beam. The spectral element code ELSE, developed at CRS4 and specifically adapted to the model at hand, has been used to solve the coupled thermal-elastic problem. The static stresses as well as the dynamic stress wave propagation in the diluter blocks are simulated up to a time sufficient to identify the different phenomena involved.

All the blocks of both TPSG4 and TPSG6 were analysed. The blocks are made of three different materials: an isotropic polycrystalline graphite, a titanium base alloy (TA6V) and the Nickel base INCONEL 718 alloy.

The primary proton beam hitting the target consists in 4 x 72 x 1.7 10^{11} protons deposited in 7.86μs, the ultimate beam intensity. The beam power deposited in the blocks was calculated on the basis of the FLUKA simulation results. The beam axis is chosen coincident with the axis of one of the copper pipes of the MSE coil.

All the blocks of the two diluters have been considered separately, with no support condition applied to the blocks (the surfaces are considered free). The block surface are considered also adiabatic -no thermal exchange is included- and thermal conduction inside the block is neglected since the time scales of thermal diffusion are by far larger than the mechanical time scales. The entire thermal problem is driven by material thermal capacity. The blocks are considered at rest with an initial temperature of 20°C.

The beam power deposition on the TPSG4 blocks causes a temperature increase that is quite high in the graphite portion of the diluter, as well as in the titanium and INCONEL blocks.

The temperature increase is high in the blocks at the first end of the diluter: it is maximum for the 2nd block, where it reaches 650ºC, and then decreases in the rest of the blocks; the maximum temperature increase in the 10th graphite block is lower than 200ºC. Along the beam axis the beam power density reduces meanwhile the cross section area on which energy is deposited widens.

The change in the material properties causes a new peak in both the titanium and INCONEL blocks, where the maximum temperature increase recorded is close to 630ºC and 450ºC respectively. This sudden temperature increase causes the rise of thermal stresses that are propagated in the block as stress waves. All the blocks of the TPSG4 have been investigated to check if the stresses may be dangerous for the material safety.

The Stassi failure criteria has been adopted, and the maximum value of the ratio between the Stassi tensile equivalent stress and the tensile strength of the material at the point temperature is recorded during the simulation, providing a map of the maximum stresses in each point of each block.

The stress values are a function not only of the magnitude of the temperature increase but also of the steepness of the radial temperature distribution and of the beam focus position in the block.

It turns out that the most stressed graphite block is not the 2nd, but the 6th. In this block there are points where the equivalent stress results slightly higher than the tensile rupture value; the load conditions cannot therefore be considered safe for the material integrity.

The maximum value of the Stassi ratio reaches 1.26 for the titanium block and 1.05 for the INCONEL block. In both cases this ratio is higher than unity, implying the risk of material failure (for the titanium block in particular).

Since the beam hitting position may influence the stress values in the blocks, we decided to check if a different position of the beam axis may cause higher stassi ratios. We analyzed the titanium and the 2nd graphite block (where the maximum energy deposition was found). The maximum value of the Stassi ratio was found to become greater than 1.5 for the titanium and 1.36 for graphite.

The desired safety factor for this simulation was 1.5 as a minimum, corresponding to a stress ratio of 0.67 as a maximum. The values found clearly exceed this limit. Considering the beam in the original position, on the basis of titanium results the beam intensity should be reduced approximately at least by a factor 1.5 x 1.26 = 1.9, to fall within the safety limit. If we consider the different possible position of the beam axis, the beam intensity should be reduced by a factor 2.2 with respect to the ultimate beam intensity.

The temperature increase due to the beam power deposition on the TPSG6 is similar to that found on the TPSG4 blocks; higher values are found on the graphite blocks and lower values on the titanium and INCONEL blocks.

The maximum value of the temperature increase is in the 1st graphite block, where it is greater than 720ºC; it is still high for the 2nd and monotonically decays to less than 200ºC for the last block.

The different material properties cause new peaks to appear in the titanium and INCONEL blocks, where the maximum temperature increase is 346ºC and 244ºC.

As for the TPSG4, stress wave propagation has been investigated. Based on the Stassi strength criterion, a map of the maximum equivalent stress found in each point during the simulation has been calculated.

The resulting stresses are again related to the maximum value of the temperature increase but also to the radial profile of the energy deposition and to the beam focus position.

The area of the deposited energy widens along the beam trajectory, and maximum stresses are not necessarily found in the block where maximum temperature increase is reached.

Concerning the graphite, the most critical conditions are found for the initial blocks; for some points of the 2nd block, in particular, the ratio between the Stassi tensile equivalent stress and the graphite rupture strength almost reaches 1.5.

Lower stresses are found in the titanium and INCONEL blocks, for which the simulated maximum value of the Stassi stress ratio is respectively 0.64 and 0.60, both below unity. The safety factor against rupture in the ultimate load condition results 1.55 for the 1st titanium block and 1.66 for the 1st INCONEL block, therefore over the minimum safety factor required.

The stresses found on the graphite blocks are very high: the peak value is found in a small portion of the block, but values near or over unity are visible for a wider portion. On the basis of the maximum stress found, the beam intensity should at least be divided by a factor of 1.46 x 1.5 = 2.2 with respect to the ultimate beam intensity, to fall below the minimum safety factor.

The reduction factor for the beam intensity has been calculated on the basis of a direct linear proportion between the beam power and the resulting stresses; this is correct if material properties were constant as a function of temperature.

Since the most significant variation of the material properties with temperature is an increase of the thermal capacity, the reduction factors should be considered as lower bound approximations; temperature reduction will be lower than the corresponding reduction of the beam intensity.

Additional simulations were run to verify the reduction factor.

With reference to the TPSG4 with the beam in the “design” position, and to the titanium block in particular, it results that the beam intensity must be reduced by a factor 2.2 in order to have a maximum temperature increase of 310ºC and maximum Stassi ratio of 0.52.

For the TPSG6 and the 2nd graphite block it is necessary to reduce the beam intensity of a factor 2.6. The maximum temperature increase is reduced to 305ºC and the maximum Stassi stress ratio to 0.64.

7. REFERENCES

[1] B. Goddard, P. Knaus, G. Schröder, W. Weterings, J. Uythoven, The New SPS Extraction Channel for LHC and CNGS, CERN-SL-2000-036 BT, July 2000.

[2] B. Goddard, P. Knaus, Beam Loss Damage in a Wire Septum, CERN-SL-2000-035 BT, July 2000.

[3] G. Ferioli, B. Goddard, P. Knaus, J. Koopman, Energy Deposition in a Septum Wire, CERN-SL-2001-029 MD, July 2001.

[4] B. Goddard, E. Carlier, P. Knaus, J. Uythoven, Equipment Protection Issues for Fast Extraction from SPS to LHC, Proc. of PAC2001, Chicago, 2001.

[5] B. Goddard et al., Transient Thermo-Mechanical Analysis of the TPSG4 Beam Diluter, CERN-SL-2002-060 ECT and refs. therein, December 2002.

[6] F. Casadei, G.Fotia, E. Gabellini, F. Maggio and A. Quarteroni, A mortar spectral/finite element method for complex 2D and 3D elastodynamic problems, Comput. Methods Appl. Mech. Energ., 191 (2002), 5119-5148

[7] L. Massidda and F. Mura, Thermal and mechanical analyses of the LHC injection beam stopper (TDI), CRS4 –TECH-REP, (2003)

[8] L. Massidda and F. Mura, Dynamic structural analysis of the TCDS Collimator, CRS4 –TECH-REP, (2004)

[9] Y. Kadi, Energy Deposition on TPSG4 and TPSG6 Protection Elements, SLI Technical Meeting, CERN, Geneva, June 2004.

[10] A. Fassò, A. Ferrari, P.R. Sala, Electron - photon transport in FLUKA status, Proc. of the Monte Carlo 2000 Conference, Lisbon, October 23-26 2000, A. Kling, F. Barão, M. Nakagawa, L. Távora, P. Vaz eds., Springer-Verlag Berlin, p. 59 - 164 (2001).

[11] A. Fassò, A. Ferrari, J. Ranft, P.R. Sala, FLUKA: Status and Prospective for Hadronic Applications, Proc. of the Monte Carlo 2000 Conference, Lisbon, October 23-26 2000, A. Kling, F. Barão, M. Nakagawa, L. Távora, P. Vaz eds., Springer-Verlag Berlin, p. 955-960 (2001).